Am J Physiol Lung Cell Mol Physiol 295: L54–L60, 2008.
First published May 16, 2008; doi:10.1152/ajplung.00475.2007.

Localized elasticity measured in epithelial cells migrating at a wound edge using atomic force microscopy

Ajay A. Wagh,[1] Esra Roan,[3] Kenneth E. Chapman,[1] Leena P. Desai,[1] David A. Rendon,[2] Eugene C. Eckstein,[3] and Christopher M. Waters[1,2]

Departments of [1]Physiology and [2]Biomedical Engineering, The University of Tennessee Health Science Center, and [3]Department of Biomedical Engineering, The University of Memphis, Memphis, Tennessee

Submitted 16 November 2007; accepted in final form 8 May 2008

Wagh AA, Roan E, Chapman KE, Desai LP, Rendon DA, Eckstein EC, Waters CM. Localized elasticity measured in epithelial cells migrating at a wound edge using atomic force microscopy. *Am J Physiol Lung Cell Mol Physiol* 295: L54–L60, 2008. First published May 16, 2008; doi:10.1152/ajplung.00475.2007.—Restoration of lung homeostasis following injury requires efficient wound healing by the epithelium. The mechanisms of lung epithelial wound healing include cell spreading and migration into the wounded area and later cell proliferation. We hypothesized that mechanical properties of cells vary near the wound edge, and this may provide cues to direct cell migration. To investigate this hypothesis, we measured variations in the stiffness of migrating human bronchial epithelial cells (16HBE cells) ~2 h after applying a scratch wound. We used atomic force microscopy (AFM) in contact mode to measure the cell stiffness in 1.5-μm square regions at different locations relative to the wound edge. In regions far from the wound edge (>2.75 mm), there was substantial variation in the elastic modulus in specific cellular regions, but the median values measured from multiple fields were consistently lower than 5 kPa. At the wound edge, cell stiffness was significantly lower within the first 5 μm but increased significantly between 10 and 15 μm before decreasing again below the median values away from the wound edge. When cells were infected with an adenovirus expressing a dominant negative form of RhoA, cell stiffness was significantly decreased compared with cells infected with a control adenovirus. In addition, expression of dominant negative RhoA abrogated the peak increase in stiffness near the wound edge. These results suggest that cells near the wound edge undergo localized changes in cellular stiffness that may provide signals for cell spreading and migration.

wound healing; ventilator-induced lung injury; Rho-GTPases

BECAUSE THE AIRWAY EPITHELIUM provides the interface between the outside environment and the body, it is vulnerable to injury from pollutants, infectious agents, and mechanical trauma. When injury to the epithelium occurs, it is important to rapidly restore the integrity of the barrier to prevent further infection or damage. The normal process of repair of airway epithelial cells, as studied in cell culture (3, 5, 26, 28, 32–35), animal studies (6, 8, 12, 19, 20), and more recently in humans (10), involves a coordinated series of events that include the establishment of a provisional matrix, dedifferentiation of nearby secretory and ciliated cells, rapid flattening and spreading of these cells, migration into the wounded area to cover the surface, and later proliferation and differentiation of cells to reestablish the functional epithelium (9, 11). The very early stages of epithelial restitution involving cell spreading and migration occur within hours of injury, and these processes necessitate substantial remodeling of cell structure. In addition, the restitution process in epithelial cells involves coordinated movement of a sheet of cells rather than cells migrating individually.

The dynamic remodeling that occurs during cell spreading and migration relies on the establishment of directional polarity of the migrating cells and extension of protrusions in the direction of migration (15, 16, 23). These protrusions can take place in the form of broader lamellipodial extensions or long and narrow filopodia. A repetitive process ensues in which the protrusions form adhesions to the substrate, rearward adhesions are disassembled, and contractile mechanisms pull the cell forward. Intrinsic to these processes is the carefully controlled remodeling of cytoskeletal structures at specific locations within the cell. Actin filament remodeling, formation and turnover of adhesion sites, and actomyosin contraction are regulated in part by members of the Rho family of small GTPases (13, 31), and we (3) previously demonstrated that an imbalance in the activity of RhoA or Rac1 can disrupt normal repair mechanisms in airway epithelial cells. Because of its prominent role in spatially regulated actin-myosin contractile processes that are essential for the cells to generate the forces necessary to pull forward during cell migration, either increasing or decreasing RhoA activity caused changes in actin distribution and resulted in significantly slower epithelial repair. Similarly, decreased Rac1 activity (by expression of dominant negative Rac1) caused decreased lamellipodial extensions and slower cell migration. Our results suggested that the coordinated movement of epithelial cell sheets required tightly regulated RhoA and Rac1 activity that normally vary spatially from the leading edge to the trailing edge.

Although it is well-recognized that spatial variations in the localization and activity of these and other signaling molecules are important for the coordination of cell migration, the relationship between these dynamic processes and the local mechanical properties of the cells are less well-understood. Raucher and Sheetz (22) manipulated membrane tension by changing phospholipid composition or by osmotically swelling cells and found that lamellipodial extension rates were decreased with increased membrane tension. They suggested that membrane tension may regulate the actin polymerization rate during lamellipodial extension. Compared with cells adhered to a stiff substrate, cells adhered to softer substrates exhibit less organized actin networks and weaker focal adhesions and

Address for reprint requests and other correspondence: C. M. Waters, Dept. of Physiology, The Univ. of Tennessee Health Science Center, 894 Union Ave., Rm. 426, Memphis, TN 38163-0001 (e-mail: cwaters2@utmem.edu).

The costs of publication of this article were defrayed in part by the payment of page charges. The article must therefore be hereby marked "*advertisement*" in accordance with 18 U.S.C. Section 1734 solely to indicate this fact.

generate less tension (7). Using force applied to the cell body using a microneedle or uniaxial substrate distention, Kaverina and colleagues (14) demonstrated increased polymerization of microtubules toward adhesion sites under elevated stress. We (27, 29) previously demonstrated that mechanical stretch and compression significantly decreased cell migration and wound closure of airway epithelial cells. However, little is known about how local mechanical properties vary during cell migration (15, 17, 18, 24). We hypothesized that local mechanical properties change during airway epithelial cell migration either as a signal to coordinate cell migration or in response to structural rearrangements that occur in the cells. In this study, we used atomic force microscopy (AFM) to examine the localized mechanical stiffness in cells far away from a wound edge and in cells migrating at the wound edge 2 h after wounding. In addition, we compared these findings with measurements in cells expressing a dominant negative form of RhoA (DN-RhoA).

MATERIALS AND METHODS

Cell culture. A cell line of human airway epithelial cells, 16HBE cells (generously donated by Dr. D. Gruenert from the University of California, San Francisco), were used for all experiments. The cells from a T-flask were trypsinized and plated on 35-mm plastic petri dishes. The cells were grown in DMEM containing 10% FBS at 37°C with 5% CO_2 until confluent in 35-mm tissue culture-treated dishes.

Adenoviral expression. Replication-deficient (E-1 deleted) recombinant type 5 adenoviruses expressing enhanced green fluorescent protein (EGFP) and dominant negative RhoA (T19N-RhoA or DN-RhoA) were infected in 16HBE cells (3). Adenoviruses were amplified using human embryonic kidney (HEK-293) cells and purified using an adenovirus purification kit (Clontech, Palo Alto, CA). Adenoviral titers were determined via a standard procedure by measurement of their cytopathic effect in HEK-293 cells and expressed in 16HBE cells. When cells were ~75% confluent, they were exposed to an adenovirus expressing either enhanced EGFP (used as a control) or DN-RhoA and incubated for an additional 24 h in serum-free media. After 24 h, the medium from the transfected dishes was removed and replaced with fresh serum-free medium. Initial studies demonstrated that EGFP-expressing cells exhibited similar mechanical properties and wound healing characteristics as uninfected cells (data not shown), and EGFP-expressing cells were compared with DN-RhoA-expressing cells in all subsequent studies.

Epithelial wound healing. Once confluent (48 h after transfection), cells were wounded by "scratching" a pipette tip (~750 μm in diameter) linearly across the confluent layer to create the wounded model. This scratch wound models injury that may occur due to direct trauma, atelectrauma (collapse and reopening of airways), and acid injury. Following wounding, cells were then rinsed using PBS, and bicarbonate-free DMEM was added again to the samples before transport to the atomic force microscope. DMEM was then aspirated, and the cells were rinsed with PBS. After rinsing, the dish was placed on the Digital Instruments (DI) Bioscope (Veeco Metrology, Santa Barbara, CA), and PBS was added to sustain the cell layer during the AFM analysis. The AFM measurements were made ~2 h after wounding the monolayer for each set of experiments to ensure that the cells had begun to migrate and spread. The wound healing and the measurements occurred at room temperature (~25°C).

AFM. A DI Bioscope was used to obtain images and force/elasticity measurements on the 16HBE cells used in these experiments. Very soft cantilevers with spring constants of about 0.01 N/m and tip half-opening angle of ~35° (Microlever/Sharp Microlever; TM Microscopes, Santa Clara, CA) were used in contact mode on the cells. To conveniently position the AFM tip above the cells, the AFM piezo head was placed on an inverted optical microscope (Nikon Diaphot 200). Imaging was done in contact mode exclusively using a fluid cell. HEPES-buffered PBS was added to the dish once the piezo head was in position over the cells and the cells were in focus under the inverted microscope. Using a scan rate of 7 Hz, the collection of each force-volume image took ~25 min, and a new calibration curve was taken for each scan field. Elastic moduli were derived from the force curves obtained from force-volume imaging done using DI software v. 5.13 (21). A force-volume image is one that is composed of force curves obtained at each location in the scan. Elastic moduli were obtained from the force curves using Sneddon's modification of the Hertzian model of elastic indentations (24, 30). Briefly, the applied loading force, F, is related to the cantilever deflection, d, by the spring constant, k,

$$F = k \cdot d = k \cdot (z - \delta) \quad (1)$$

where z is the piezo movement or height and δ is the indentation depth. Sneddon's modification of the Hertzian model for the elastic indentation of a cone into a sample relates the loading force to the Young's modulus of the material (or elasticity), E, according to

$$F = (2/\pi) \times \tan(\alpha) \times E/(1 - \nu^2) \times \delta^2 \quad (2)$$

where α is the AFM tip half-opening angle (35°), and ν is the Poisson ratio of the sample (assumed to be 0.5). *Equations 1* and *2* were then used to relate the piezo movement, z, to the cantilever deflection, d, as follows

$$z - z_o = d - d_o + \sqrt{\frac{k(d - d_o)}{\left(\frac{2}{\pi}\right)\left(\frac{E}{1 - \nu^2}\right)\tan\alpha}} \quad (3)$$

where z_o and d_o are the initial values. Assuming d_o to be 0 at the contact point, *Eq. 3* was then fit to the experimental data by varying the contact point, z_o, and the modulus, E. Force curves were analyzed and elasticity maps were generated using a custom-developed MATLAB program. Only the approach curves were used in the analysis, and data were analyzed only in the low force region between 10 and 40 nm deflection. A Simplex algorithm was used within MATLAB to minimize the sum of squared differences between the experimental curve and the predicted curve in the range of 10–40 nm deflection. Deflection values in the range below 10 nm were not used because of greater noise in the data potentially due to interactions between the tip and the substrate. Deflection values greater than 40 nm were not used because of the nonlinear properties of the cells at the higher forces. The number of data points within this range was typically 3–6. In some cases, the regression routine did not converge on a solution, and elasticity values for these locations were not used. To compare the elasticity maps to the topology of the cells, we also measured the height of the cells relative to the lowest contact point in a given field.

Force-volume images were taken with 32 force curves/line and with 32 points/curve. Fifty micrometer-by-fifty micrometer images were taken at the wound edge and at locations at least 3.75 mm away from the wound edge. Each force curve corresponds to a pixel size of 50/32 or 1.56 μm. Cells far from the wound edge (>3.75 mm) were assumed to maintain properties of unwounded cells. Elasticity values at each point were used to construct two-dimensional elasticity maps. Four or five scan regions from at least three different experiments for each condition were used for comparisons.

Statistical analysis. All values are presented as means ± SE or as the median value. Statistical analysis was performed with the SigmaStat statistical package (v. 3.5; Jandel Scientific, San Rafael, CA). Because the data were not normally distributed, Kruskal-Wallis one-way ANOVA on ranks was used, and Dunn's method for comparison of ranks was used to compare treatments. Significant differences were determined based on a threshold of $P < 0.05$.

RESULTS

Elastic modulus was heterogeneous in 16HBE airway epithelial cells. Figure 1 shows AFM deflection images of 16HBE cells far away from the wound edge (>3.75 mm) and cells at the wound edge. Note that the cells in Fig. 1*B* were migrating into the wounded area indicated by the arrows. To determine the elasticity at each location in a scan area, we obtained force curves as described in MATERIALS AND METHODS. Figure 2*A* is an example of a force curve showing the relationship between the piezo movement (or *z*-height) and the cantilever deflection (d). As indicated in the figure, the region between 10 and 40 nm of deflection was used for the analysis of the curve. Using the relationships described in MATERIALS AND METHODS, this curve resulted in the calculation of an elastic modulus of 3.26 kPa. This represents one point in an elasticity map. Figure 2*B* shows a representative elasticity map in a region of cells far from the wound edge (preliminary studies indicated that elasticity values at this distance from the wound edge, >3.75 mm, were similar to those obtained in confluent 16HBE cells that were not wounded; data not shown). As shown in the image, the elastic modulus values varied substantially within a given field, indicating the heterogeneity of cell stiffness. Figure 2*C* shows the topology of the same field as shown in Fig. 2*B* by plotting the height at each location relative to the lowest contact point in the field. Taken together, these plots suggest that, in general, higher stiffness was observed in regions outside of the central nuclear regions. Table 1 summarizes the data obtained from five different fields for control cells. The elasticity values did not follow a Gaussian distribution, but median and quartile measurements were consistent in the different fields: 75% of the measurements were less than 10 kPa, and the median value for all measurements was 2.4 kPa. Figure 2*D* shows elasticity values obtained from five different fields as a function of scan position across the field. Both mean and median elasticity values were consistent along a scan line.

Expression of DN-RhoA decreased cell stiffness. We (3) previously demonstrated that expression of DN-RhoA in 16HBE cells resulted in a decrease in F-actin stress fibers and inhibition of wound healing. To determine whether expression of DN-RhoA caused a decrease in cell stiffness, we infected cells with an adenovirus expressing DN-RhoA 48 h before measurements of elastic modulus. Figure 3 shows a representative elasticity map of cells far away from the wound edge and data summarized from five fields as a function of position across the scan. As in the case of control cells, the elasticity values were not normally distributed, but Table 1 shows that the median elasticity for cells expressing DN-RhoA was significantly lower than in control cells. Seventy-five percent of the measurements in DN-RhoA cells were lower than 3.5 kPa compared with 10.0 kPa for control cells.

Mechanical stiffness varied significantly near the wound edge. To determine whether cell stiffness varied as a function of distance from the wound edge in migrating cells, scratch wounds were made, the cells were rinsed, and elasticity maps were obtained ~2 h after wounding. Figure 4 shows a representative elasticity map at a wound edge and data summarized from four different fields as a function of distance from the wound edge. Within the first 5 μm from the edge of the wound, the median elastic modulus was significantly lower than the median value obtained far from the wound edge. After 10 μm, the elasticity significantly increased above control values to a peak value of ~9 kPa and then decreased again to control levels after 20 μm. These results indicate a softening of the cells at the leading edge and a stiffening of the cells between 10 and 20 μm from the edge.

DN-RhoA reduced the increase in stiffness at the wound edge. To determine whether the stiffening of cells near the wound edge was dependent on contractile mechanisms involving RhoA, we measured the stiffness as a function of position in DN-RhoA-expressing cells. Figure 5 shows that elasticity values were significantly decreased within the first 3 μm of the wound edge, and there were regions of increased stiffness at ~20 and 40 μm from the edge, but the substantial increase observed in control cells was largely abrogated.

DISCUSSION

We (27, 29) previously demonstrated that cyclic mechanical stretch inhibited cell migration and wound healing of airway epithelial cells. Because both cell spreading and cell migration velocity were decreased by mechanical stretch in these studies, we hypothesized that these changes were potentially due to disruption of mechanical cues necessary for organized and efficient wound closure. In the current study, we sought to determine whether the mechanical properties of cells varied spatially during cell migration at a wound edge. We first investigated the distribution of elasticity in cells far from the wound edge and observed substantial heterogeneity in a given field, but median values were consistently less than 5 kPa (Fig. 2). Because of the substantial variation in elasticity values in regions outside the nucleus, the mean values did not follow a Gaussian distribution and were consistently higher than median values. Although Fig. 2 suggests the possibility that higher

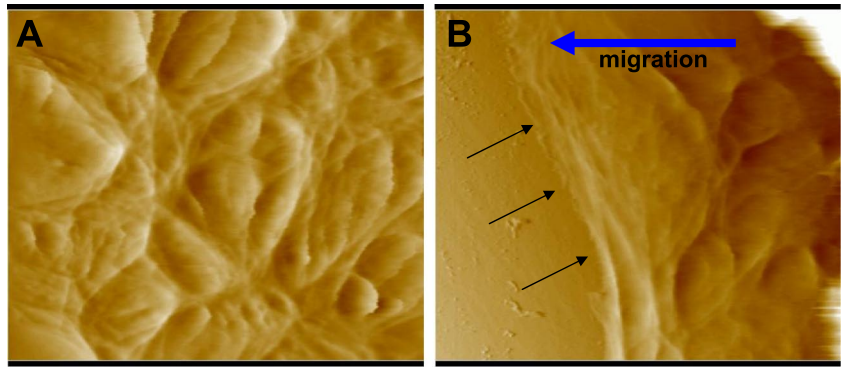

Fig. 1. Atomic force microscopy height images of control human bronchial epithelial cells (16HBE cells) infected with adenovirus expressing enhanced green fluorescent protein (EGFP) at a distance far from the wound edge (>3.75 mm; *A*) and at the wound edge ~2 h after wounding (*B*). Black arrows in *B* indicate the wound edge as cells are migrating from right to left (indicated by blue arrow). Each image shows a 50- × 50-μm field.

modulus values were observed in junctional regions, we did not independently identify these regions. We next investigated the mechanical stiffness of 16HBE cells at the leading edge of a wound and found that elasticity was significantly decreased compared with cells far from the wound edge (Fig. 4). This stiffness then increased dramatically between 10 and 20 μm from the leading edge before returning to values similar to unwounded regions. These results demonstrate that while there is substantial heterogeneity in the stiffness characteristics of cells in an unwounded monolayer, there is a coordinated change in the mechanical properties of cells at the leading edge of a wound. The softening of the cells at the leading front and an increase in stiffness 10–20 μm back is consistent with the relaxation of focal adhesions as cells are spreading and the actin remodeling and contraction of the cells as they attempt to pull forward. The decrease in elasticity at distances >30 μm from the edge may suggest relaxation of the cells at the trailing edge. In future studies, we will attempt to relate topographical and structural features of individual cells to elasticity mapping. When we disrupted cytoskeletal remodeling and inhibited actomyosin contraction by expressing DN-RhoA, the overall stiffness of the cells decreased (Table 1), and the dramatic spatial variation in stiffness at the wound edge was removed (Fig. 5).

Our results are consistent with the studies by Rotsch and colleagues (24, 25) who examined the mechanical properties of fibroblasts. They also measured substantial heterogeneity in the elastic moduli of fibroblasts with a range of values similar to our measurements in 16HBE cells. They observed a significant reduction in the average elastic modulus of fibroblasts treated with F-actin disrupting drugs (such as cytochalasins B and D and latrunculin), but disruption of microtubules had no effect on the elastic modulus (25). When examining the leading edge of single fibroblasts, they found that motile fibroblasts had lower stiffness than quiescent fibroblasts within the first 4 μm of the edge (24). However, they measured elastic moduli only in the initial lamellipodial region in this study. As in the studies by Rotsch and colleagues (24, 25), we analyzed our data using the approach portion of the force curves. The retraction curves

Table 1. *Comparison of elastic modulus values in regions far (>3.75 mm) from the wound edge*

Value	Control	DN-RhoA
Mean	8.70 kPa	5.12 kPa
SD	16.39 kPa	10.47 kPa
SE	0.23 kPa	0.15 kPa
n	5,120	5,120
Median	2.40 kPa	1.33 kPa*
25th percentile	0.82 kPa	0.76 kPa
75th percentile	10.02 kPa	3.52 kPa

Elastic modulus values are taken from 5 different fields for each condition. *$P < 0.05$. Data sets did not have equal variance and were not normally distributed. Therefore, a nonparametric comparison based on ranks was used (Dunn's method). DN-RhoA, a dominant negative form of RhoA.

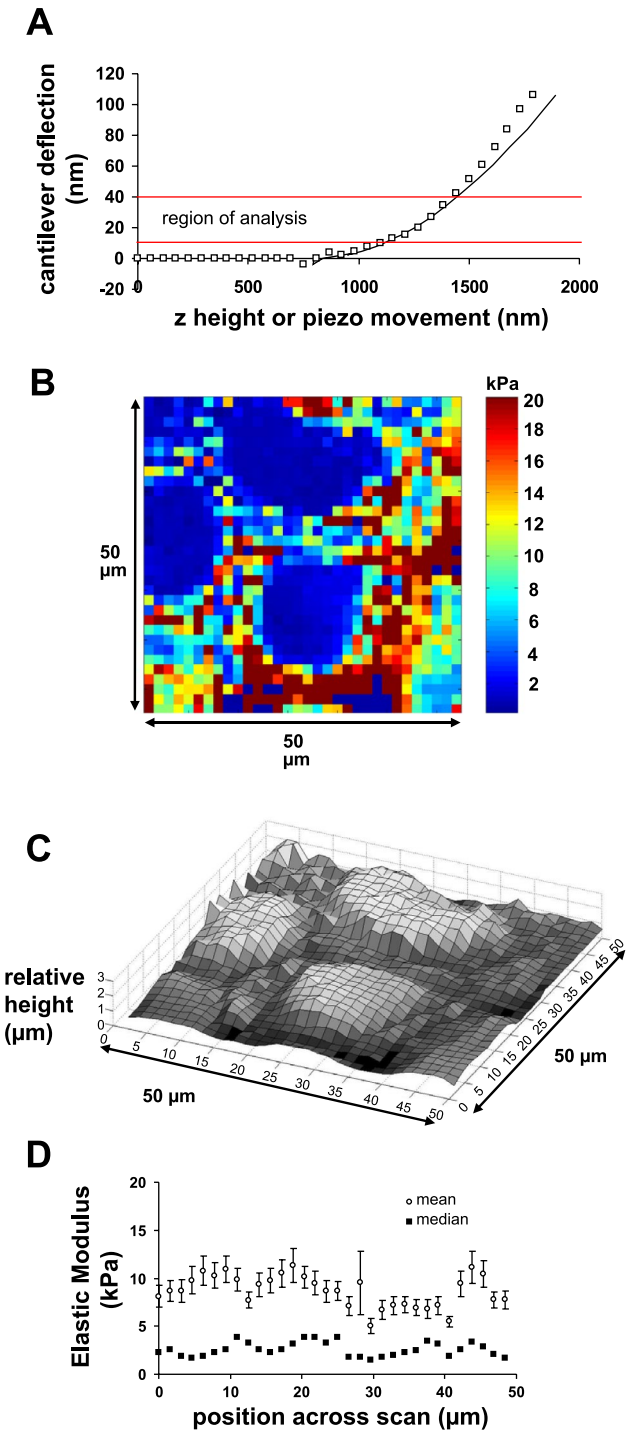

Fig. 2. Distribution of elastic modulus values in control (EGFP-expressing) 16HBE cells. *A*: example of a force curve used to calculate elastic modulus. Plot of *z*-height vs. cantilever deflection. Symbols represent experimental data, while the solid line indicates the best fit of the Hertz model to the data within the range of 10–40 nm deflection (indicated by solid red lines). The elastic modulus derived from this curve was 3.26 kPa, and the r^2 value was 0.9809. *B*: representative elasticity map of 16HBE cells at a distance >3.75 mm from a wound edge. The color map indicates the modulus of elasticity (in kPa) evaluated using force curves generated at each point in the field. Each pixel represents a 1.56- × 1.56-μm region of the field. The image shows a 50- × 50-μm field. *C*: relative height of cells in the same field as shown in *B*. This measurement does not give the absolute height but rather the height relative to the lowest contact point in the field. *D*: elastic modulus values summarized from 5 different fields as a function of the position across a scan line. Mean values (open squares) ± SE are shown as well as median values (closed squares). Each data point represents the median or mean value calculated from vertical scan lines from the same location in 5 different fields ($n = 5 \times 32$ values for each data point).

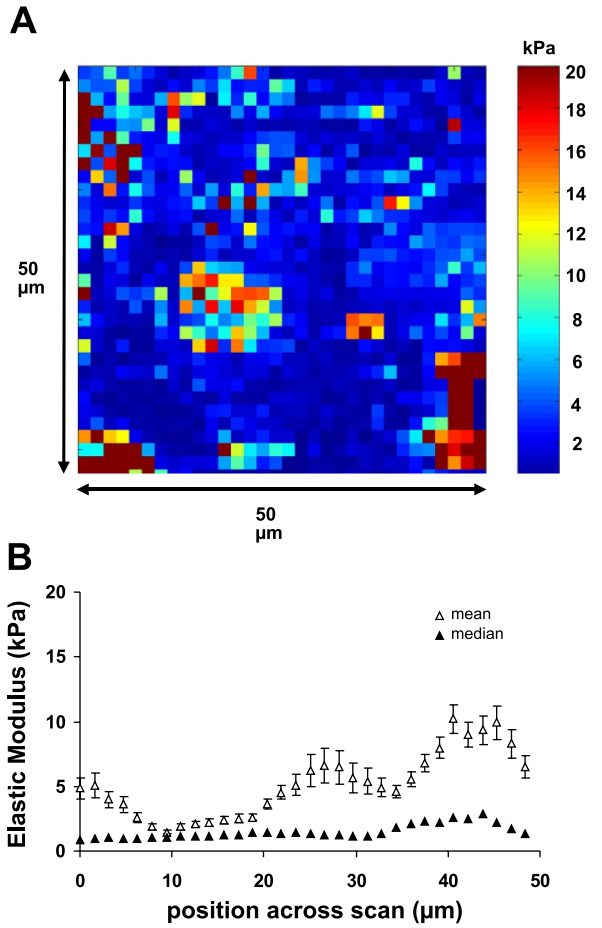

Fig. 3. Expression of a dominant negative form of RhoA (DN-RhoA) caused softening of 16HBE cells. *A*: representative elasticity map of DN-RhoA-expressing 16HBE cells at a distance >3.75 mm from a wound edge (as in Fig. 2). *B*: elastic modulus values in DN-RhoA-expressing cells summarized from 5 different fields as a function of the position across a scan line. Mean values (open squares) ± SE are shown as well as median values (closed squares). Each data point represents the median or mean value calculated from vertical scan lines from the same location in 5 different fields ($n = 5 \times 32$ values for each data point).

sometimes showed indications of adhesive interactions between the probe tip and the cells.

Using a similar approach with scanning probe microscopy, Nagayama and colleagues (18) found that the central region of a migrating fibroblast initially stiffened compared with the central region of a stationary cell, but then the stiffness in the central region significantly decreased as the cell migrated. Kole and collaborators (15) also compared migrating and stationary fibroblasts, but they evaluated intracellular mechanics using microinjected fluorescent microbeads. They found that cells at the edge of a wounded monolayer (4 h after wounding) were less deformable (stiffer) than quiescent fibroblasts. To examine localization of the mechanical properties in these cells, they compared the central region of the cells (30-μm radius surrounding the nucleus) with the rest of the cell. They found that the outer region of migrating cells was stiffer than the central region, while the stiffness in the perinuclear region of quiescent cells was similar to the outer region. Although we did not distinguish individual cells, since epithelial cells migrate as a coordinated sheet, our results are in general agreement with those of Kole et al. (15) since we also measured stiffening of the cells within 10–20 μm of the leading edge. However, our approach allowed localization of the changes in elastic modulus as a function of the distance from the edge. The profile of elastic modulus at the leading edge of migrating individual keratocytes, measured using AFM, demonstrated increased stiffness at the leading edge that gradually decreased toward the center of the cells (17). These results differ somewhat from our findings, but this may be related to the rapid migration rate of keratocytes and the difference between the migration of individual cells and cell sheets. It is unclear what advantage would be gained by increased stiffness at the leading edge of a rapidly migrating cell, but if focal adhesions are being released and actin is remodeling then one might expect to have less stiff regions.

As described previously, there are limitations to the AFM approach for measurements of mechanical properties of cells. First, the use of the Hertz model to evaluate the elastic modulus is a simplification of a complex mechanical system (1, 24, 25).

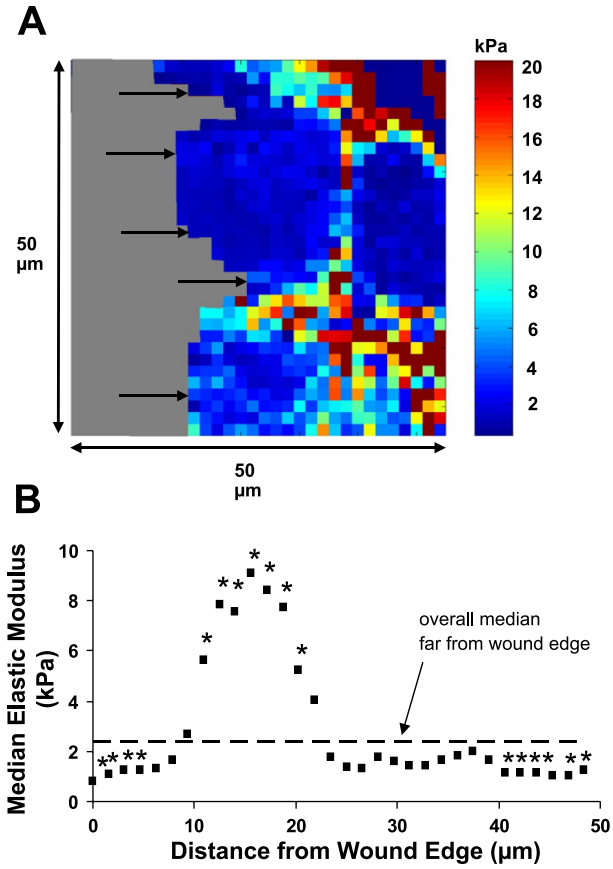

Fig. 4. Cell stiffness varies as a function of distance from the wound edge in 16HBE cells. *A*: representative elasticity map of control 16HBE cells at a wound edge 2 h after wounding. Arrows indicate the wound edge as cells were migrating from right to left. Gray regions indicate plastic substrate. *B*: median elastic modulus values as a function of distance from the wound edge were summarized from 4 different fields. Each data point represents the median value calculated from a fixed distance in the *x*-direction along a scan line from 4 fields ($n = 4 \times$ the number of values measured at that distance from the edge). Data points at the greatest distance from the wound edge had the fewest measurements because the fields always contained some area without cells. The dashed line indicates the median value from control cells far away from the wound edge (2.4 kPa), and the asterisks indicate a significant difference from this value ($P < 0.05$).

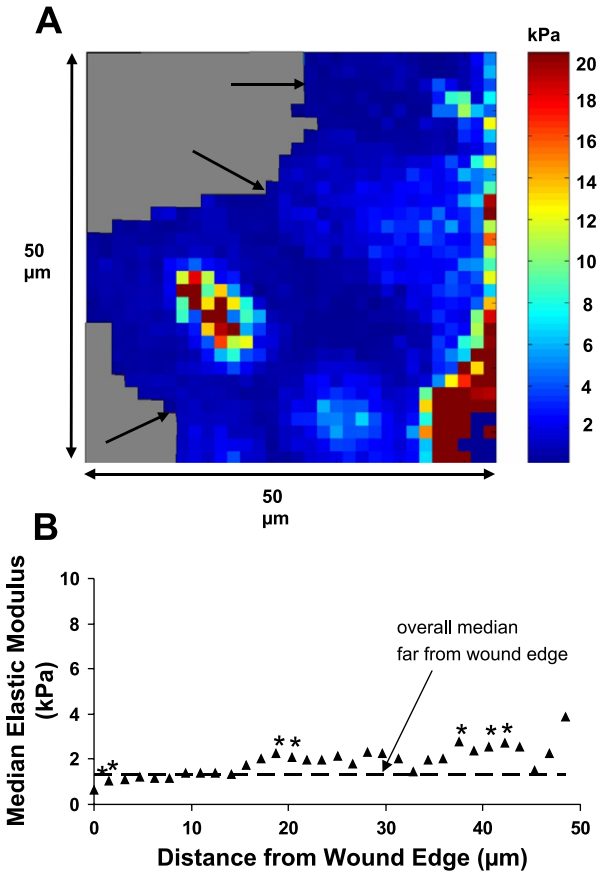

Fig. 5. Expression of DN-RhoA reduced the increase in cell stiffness near the wound edge. *A*: representative elasticity map of 16HBE cells expressing DN-RhoA at a wound edge 2 h after wounding. Arrows indicate the wound edge as cells were migrating from right to left. Gray regions indicated plastic substrate. *B*: median elastic modulus values as a function of distance from the wound edge were summarized from 5 different fields. Each data point represents the median value calculated from a fixed distance in the *x*-direction along a scan line from 5 fields ($n = 5 \times$ the number of values measured at that distance from the edge). The dashed line indicates the median value from cells expressing DN-RhoA far away from the wound edge (1.33 kPa), and the asterisks indicate a significant difference from this value ($P < 0.05$).

This model assumes that elastic deformation occurs between two homogeneous smooth surfaces that are isotropic. Because of the variability of materials and structures within cells, they are clearly not isotropic. However, we limited our analysis to the linear regions of the force curves to minimize the effects of nonlinear properties of the cells. The model also assumes that the sample is infinitely thick and uniformly elastic, and this assumption is clearly untrue when the height of the cell is comparable to the size of the probe tip, for example when lamellipodial extensions are very thin (200–300 nm). Under these conditions and with higher loading forces, the probe tip will be influenced by the stiffness of the underlying substrate, and the estimated elastic modulus is considered as an upper limit. Although these serious limitations prevent determining highly precise values for the modulus, they do not preclude comparisons of the spatial distribution of apparent moduli from our data because we analyzed the low force region of the curves where the cantilever deflection was small (Fig. 2*A*, for example, between 10 and 40 nm, which corresponds with a force range of approximately 100 to 400 pN). Also, our results demonstrated lower values of elastic modulus in the thinnest regions of the cells at the leading edge rather than elevated values. Another common assumption in the use of this model is that the Poisson ratio of the cells is 0.5, but this has not been measured experimentally. With these considerations in mind, elastic modulus values obtained using this approach should be considered as an apparent elastic modulus that can be used for comparisons but may not accurately reflect the true elastic modulus of the cells. In fact, viscoelastic properties measured using other approaches, such as those using intracellular fluorescent bead tracking (15), can be orders of magnitude smaller than those measured using AFM approaches. However, each of these approaches has advantages and disadvantages, and we used the AFM approach to make measurements of the relative elastic properties with high spatial resolution at the wound edge.

Expansion of the lungs during the respiratory cycle causes lung epithelial cells to be exposed to large deforming stresses. Previous studies have demonstrated complex microrheology of lung epithelial cells with "structural disorder and metastability" that suggests a strong capability to adapt to mechanical stress (1a, 2). Measurements of the Young's modulus for two types of human-derived lung epithelial cells, A549 (alveolar) and BEAS-2B (bronchial), were comparable to our measurements (1.59 and 1.55 kPa, respectively). We did not evaluate the response of 16HBE cells to dynamic stresses in the current study, but our results do suggest complex but coordinated rearrangements of the cell mechanical properties at the leading edge of a wound. We speculate that the decrease in cell migration in response to cyclic mechanical stretch that we observed in previous studies (27, 29) may be due to disruption of these complex rearrangements. These rearrangements are likely coordinated with signaling through Rho GTPases. We previously demonstrated that 16HBE wound closure was regulated by both RhoA and Rac1 signaling and that expression of either constitutively active or DN-RhoA inhibited wound closure (3). These findings are consistent with the current study in that expression of DN-RhoA significantly reduced the increase in stiffness near the leading edge of the wound. These results support the hypothesis that signaling pathways that are involved in structural rearrangements, such as those involving RhoA, are necessary to regulate the mechanical stiffness spatially. We can not, however, rule out the possibility that these variations in localized elasticity, in turn, lead to further spatial regulation of these signaling processes. Our measurement of the spatial variation of mechanical stiffness with respect to the wound edge and the blunting of this variation with DN-RhoA suggest that variations in mechanical properties at the wound edge are dependent on RhoA signaling and are important for coordinated cell migration.

ACKNOWLEDGMENTS

We gratefully acknowledge Dr. Manfred Radmacher, Dr. Sanjay Mishra, Dr. Jeremy Mao, Dr. Jae Young Rho (deceased), and Greg Koppel for their help with technical questions regarding the operation of the AFM. We also thank Lou Boykins, Sharon Frase, and Dr. Lewis Coones from the Integrated Microscopy Center at the University of Memphis for their help in using the AFM. We thank Dr. Scott Sinclair for helpful discussions regarding this manuscript.

GRANTS

This study was supported by National Heart, Lung, and Blood Institute Grant HL-064981.

REFERENCES

1. **A-Hassan E, Heinz WF, Antonik MD, D'Costa NP, Nageswaran S, Schoenenberger CA, Hoh JH.** Relative microelastic mapping of living cells by atomic force microscopy. *Biophys J* 74: 1564–1578, 1998.
1a. **Alcaraz J, Buscemi L, Grabulosa M, Trepat X, Fabry B, Farre R, Navajas D.** Microrheology of human lung epithelial cells measured by atomic force microscopy. *Biophys J* 84: 2071–2079, 2003.
2. **Berrios JC, Schroeder MA, Hubmayr RD.** Mechanical properties of alveolar epithelial cells in culture. *J Appl Physiol* 91: 65–73, 2001.
3. **Desai LP, Aryal AM, Ceacareanu B, Hassid A, Waters CM.** RhoA and Rac1 are both required for efficient wound closure of airway epithelial cells. *Am J Physiol Lung Cell Mol Physiol* 287: L1134–L1144, 2004.
4. **Dorscheid DR, Patchell BJ, Estrada O, Marroquin B, Tse R, White SR.** Effects of corticosteroid-induced apoptosis on airway epithelial wound closure in vitro. *Am J Physiol Lung Cell Mol Physiol* 291: L794–L801, 2006.
6. **Erjefalt JS, Erjefalt I, Sundler F, Persson CG.** In vivo restitution of airway epithelium. *Cell Tissue Res* 281: 305–316, 1995.
7. **Felsenfeld DP, Schwartzberg PL, Venegas A, Tse R, Sheetz MP.** Selective regulation of integrin–cytoskeleton interactions by the tyrosine kinase Src. *Nat Cell Biol* 1: 200–206, 1999.
8. **Gomperts BN, Belperio JA, Fishbein MC, Keane MP, Burdick MD, Strieter RM.** Keratinocyte growth factor improves repair in the injured tracheal epithelium. *Am J Respir Cell Mol Biol* 37: 48–56, 2007.
9. **Hackett TL, Knight DA.** The role of epithelial injury and repair in the origins of asthma. *Curr Opin Allergy Clin Immunol* 7: 63–68, 2007.
10. **Heguy A, Harvey BG, Leopold PL, Dolgalev I, Raman T, Crystal RG.** Responses of the human airway epithelium transcriptome to in vivo injury. *Physiol Genomics* 29: 139–148, 2007.
11. **Holgate ST, Holloway J, Wilson S, Bucchieri F, Puddicombe S, Davies DE.** Epithelial-mesenchymal communication in the pathogenesis of chronic asthma. *Proc Am Thorac Soc* 1: 93–98, 2004.
12. **Hong KU, Reynolds SD, Watkins S, Fuchs E, Stripp BR.** In vivo differentiation potential of tracheal basal cells: evidence for multipotent and unipotent subpopulations. *Am J Physiol Lung Cell Mol Physiol* 286: L643–L649, 2004.
13. **Horwitz AR, Parsons JT.** Cell migration–movin' on. *Science* 286: 1102–1103, 1999.
14. **Kaverina I, Krylyshkina O, Beningo K, Anderson K, Wang YL, Small JV.** Tensile stress stimulates microtubule outgrowth in living cells. *J Cell Sci* 115: 2283–2291, 2002.
15. **Kole TP, Tseng Y, Jiang I, Katz JL, Wirtz D.** Intracellular mechanics of migrating fibroblasts. *Mol Biol Cell* 16: 328–338, 2005.
16. **Lauffenburger DA, Horwitz AF.** Cell migration: a physically integrated molecular process. *Cell* 84: 359–369, 1996.
17. **Laurent VM, Kasas S, Yersin A, Schaffer TE, Catsicas S, Dietler G, Verkhovsky AB, Meister JJ.** Gradient of rigidity in the lamellipodia of migrating cells revealed by atomic force microscopy. *Biophys J* 89: 667–675, 2005.
18. **Nagayama M, Haga H, Kawabata K.** Drastic change of local stiffness distribution correlating to cell migration in living fibroblasts. *Cell Motil Cytoskeleton* 50: 173–179, 2001.
19. **Park KS, Wells JM, Zorn AM, Wert SE, Laubach VE, Fernandez LG, Whitsett JA.** Transdifferentiation of ciliated cells during repair of the respiratory epithelium. *Am J Respir Cell Mol Biol* 34: 151–157, 2006.
20. **Plopper CG, Mango GW, Hatch GE, Wong VJ, Toskala E, Reynolds SD, Tarkington BK, Stripp BR.** Elevation of susceptibility to ozone-induced acute tracheobronchial injury in transgenic mice deficient in Clara cell secretory protein. *Toxicol Appl Pharmacol* 213: 74–85, 2006.
21. **Radmacher M, Cleveland JP, Fritz M, Hansma HG, Hansma PK.** Mapping interaction forces with the atomic force microscope. *Biophys J* 66: 2159–2165, 1994.
22. **Raucher D, Sheetz MP.** Cell spreading and lamellipodial extension rate is regulated by membrane tension. *J Cell Biol* 148: 127–136, 2000.
23. **Ridley AJ, Schwartz MA, Burridge K, Firtel RA, Ginsberg MH, Borisy G, Parsons JT, Horwitz AR.** Cell migration: integrating signals from front to back. *Science* 302: 1704–1709, 2003.
24. **Rotsch C, Jacobson K, Radmacher M.** Dimensional and mechanical dynamics of active and stable edges in motile fibroblasts investigated by using atomic force microscopy. *Proc Natl Acad Sci USA* 96: 921–926, 1999.
25. **Rotsch C, Radmacher M.** Drug-induced changes of cytoskeletal structure and mechanics in fibroblasts: an atomic force microscopy study. *Biophys J* 78: 520–535, 2000.
26. **Savla U, Appel HJ, Sporn PH, Waters CM.** Prostaglandin E_2 regulates wound closure in airway epithelium. *Am J Physiol Lung Cell Mol Physiol* 280: L421–L431, 2001.
27. **Savla U, Olson LE, Waters CM.** Mathematical modeling of airway epithelial wound closure during cyclic mechanical strain. *J Appl Physiol* 96: 566–574, 2004.
28. **Savla U, Sporn PH, Waters CM.** Cyclic stretch of airway epithelium inhibits prostanoid synthesis. *Am J Physiol Lung Cell Mol Physiol* 273: L1013–L1019, 1997.
29. **Savla U, Waters CM.** Mechanical strain inhibits repair of airway epithelium in vitro. *Am J Physiol Lung Cell Mol Physiol* 274: L883–L892, 1998.
30. **Sneddon IN.** The relation between load and penetration in the axisymmetric Boussinesq problem for a punch of arbitrary profile. *Int J Eng Sci* 3: 47–57, 1965.
31. **Van Aelst L, Symons M.** Role of Rho family GTPases in epithelial morphogenesis. *Genes Dev* 16: 1032–1054, 2002.
32. **Waters CM, Savla U.** Keratinocyte growth factor accelerates wound closure in airway epithelium during cyclic mechanical strain. *J Cell Physiol* 181: 424–432, 1999.
33. **Wesley UV, Bove PF, Hristova M, McCarthy S, van der Vliet A.** Airway epithelial cell migration and wound repair by ATP-mediated activation of dual oxidase 1. *J Biol Chem* 282: 3213–3220, 2007.
34. **White SR, Tse R, Marroquin BA.** Stress-activated protein kinases mediate cell migration in human airway epithelial cells. *Am J Respir Cell Mol Biol* 32: 301–310, 2005.
35. **Zahm JM, Kaplan H, Herard AL, Doriot F, Pierrot D, Somelette P, Puchelle E.** Cell migration and proliferation during the in vitro wound repair of the respiratory epithelium. *Cell Motil Cytoskeleton* 37: 33–43, 1997.